2022 NDIA MICHIGAN CHAPTER
GROUND VEHICLE SYSTEMS ENGINEERING
AND TECHNOLOGY SYMPOSIUM
MODELING SIMULATION AND SOFTWARE (MS2) TECHNICAL SESSION
AUGUST 16-18, 2022 - NOVI, MICHIGAN

SIMULATION OF SNOW TEXTURE FOR AUTOMOMOUS VEHICLE NUMERICAL MODELING

Sergey Vecherin, Aaron Meyer, Brian Quinn, Theodore Letcher, Michael Parker

U. S. Army ERDC - Cold Regions Research and Engineering Laboratory, Hanover, NH

ABSTRACT

To advance development of the off-road autonomous vehicle technology, software simulations are often used as virtual testbeds for vehicle operation. However, this approach requires realistic simulations of natural conditions, which is quite challenging. Specifically, adverse driving conditions, such as snow and ice, are notoriously difficult to simulate realistically. The snow simulations are important for two reasons. One is mechanical properties of snow, which are important for vehicle-snow interactions and estimation of route drivability. The second one is simulation of sensor responses from a snow surface, which plays a major role in terrain classification and depends on snow texture. The presented work describes an overview of several approaches for realistic simulation of snow surface texture. The results indicate that the overall best approach is the one based on the Wiener–Khinchin theorem, while an alternative approach based on the Cholesky decomposition is the second best.

Citation: S. Vecherin, A. Meyer, J. Desmond, K. Dunn, B. Quinn, T. Letcher, M. Parker, "Simulation of Snow Roughness for Autonomous Vehicle Numerical Modeling," In *Proceedings of the Ground Vehicle Systems Engineering and Technology Symposium* (GVSETS), NDIA, Novi, MI, Aug. 16-18, 2022.

1. INTRODUCTION

Determining drivability of a route is a fundamental problem in off-road vehicle autonomy. This problem is made more challenging in cold regions by snow and ice, where characteristics of snow and ice surfaces can vary greatly due to rapidly changing factors such as snow depth, strength, density, and friction characteristics [1]. Current autonomy vehicle packages are primarily focused on the proprioception technologies, do not account for the type of snow or ice surface, and therefore are not able to adequately predict drivability on these surfaces.

As pointed out in [2], a comprehensive solution should include look-ahead sensing with terrain classification in front of the vehicle. This information can be used for optimal routing and to inform autonomous vehicle controllers, which would adapt for the upcoming driving conditions. Then, information from the look-ahead sensing will be combined with the instantaneous vehicle proprioception sensing to make fine-tuning of

autonomous systems for more robust and safe driving.

In order to reproduce a wide variety of driving conditions, numerical simulations are often used for the development of autonomy algorithms. Such simulations can provide very valuable insights and substantially reduce the time and cost of experiments as long as they reproduce realistic physics of the vehicle-terrain interaction and, for the terrain classification, realistic sensor performance.

For the vehicle-terrain interaction modeling, physics based snow models are used. Such models use physical laws that govern snow accumulation, based on the energy-mass balance, and typically require many meteorological parameters as inputs, such as energy fluxes, precipitations, humidity, sun energy radiation, wind, surface type and geometry, etc. This is approach adopted in the land surface modeling (LSM), e.g., Noah LSM developed by the National Oceanic and Atmospheric Administration (NOAA) [3, 4] and SNODAS snow model developed by the National Operational Hydrologic Remote Sensing Center (NOHRSC), which incorporated several previously developed approaches for mathematical formulation, snow dynamics, and mass-energy transport [5, 6]. Such models are useful in the studies of global climate, meteorology, and regional weather, but have limited applicability to the terrain-informed autonomous vehicles. Due to availability of the data used as required inputs in these models, the spatial resolution of their simulations is rather coarse, reaching the limit of 1 km as its finest. For vehicle autonomy, much smaller spatial scales are needed.

A physics based numerical model, which can be used to simulate snow depth on a 10 m grid, is Glen Liston's SnowModel [7]. SnowModel is a single-column model that simulates the accumulation and ablation of snow in response to meteorological forcing. Specifically, it solves the energy balance equation for the snow surface and the 1D heat transport through the snowpack. Additionally, SnowModel has a forest canopy component that simulates the effects of an overhead forest canopy on precipitation, wind speed, and radiation.

While meter spatial scales might be sufficient for estimating route drivability, such scales are not sufficient to reproduce the surface reflection of the lidars or visual appearance of the snow surface. For these tasks, even finer spatial resolution is needed [2, 8]. To address this problem, we adopted a statistical approach, in which these fine-scale variations in snow properties, e.g., snow depth, are treated as a two-dimensional (2D) random field with certain correlation properties. In the core of our approach lies a separation of a snow layer height field into the background and fine-scale fields, which are defined by the user-defined outer and inner spatial scales. The background field is thought to be modeled by one of the suitable physics-based models described above, while the fine-scale field, responsible for the texture or roughness, is modeled through the simulation of 2D correlated random processes. A complete snowfall scene, then, is obtained as a sum of the large- and small-scale fields. In this paper, several approaches for realistic simulation of snow texture are considered, compared, and suggestions are drawn for the best practical approach.

2. DATA PREPROCESSING

The data described in this paper were collected near Union Village Dam, Thetford, VT, on 11 Mar 2021. Images were collected with the R80D SkyRaider unmanned aerial system (UAS) with an integrated onboard HDZoom camera. The UAS was flown using a preprogrammed flight plan allowing overlapping images to be collected over the entire test area while imaging several key areas to include sections of roadway, fields, fabricated obstacles, and a river. An orthomosaic image was created from these photos as the first step of the photogrammetry that ultimately ends with a high-resolution (6 cm) digital elevation model of the scene. This is created by joining the overlapping smaller images for the area to create a unified image of the entire scene, which is shown in Figure 1.

Figure 1: An orthomosaic image of the data acquisition site.

As mentioned in the Introduction, the first step in the data pre-processing is a separation of the digital elevation map of the scene shown in Figure 1 into the background and fine-scale images. Such a separation is based on the desirable outer and inner spatial scales. Then, the outer scale background image can be simulated by a physics-based model, while the focus of this paper is on the modeling approaches for the fine-scale field.

The background can be estimated by various methods. The simplest one is to remove the mean elevation, which will not remove overall slope of the scene. Another possibility would be to remove a 2D trend in the elevation by fitting a plane, which would resolve the average slope issue. However, both approaches will leave in the residual fine-scale image all large features, such as hills, valleys, and natural of fabricated structures. To adequately construct the background image, we used the 2D centered moving average filtration with the spatial lags equal to the outer scale. Then, the fine scale image is obtained as a difference between the original and filtered image. Figures 2a and 2b show the filtered and fine-scale images for the outer scale of 2 m.

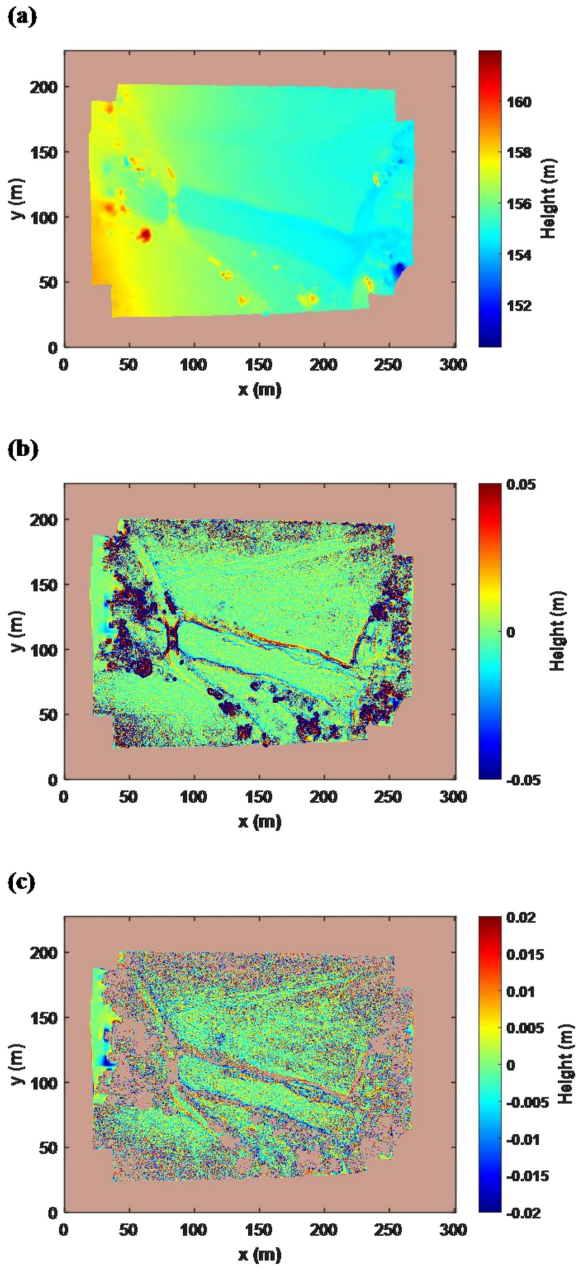

Figure 2: Image preprocessing. (a) Digital elevation model of the background for the snow scene shown in Figure 1. (b) Fine-scale residual image. (c) Filtered image shown in Figure 2b with outliers removed.

As one can see in Figure 2b, the fine-scale image contains many outliers caused not by snow texture, but by large-scale natural and fabricated features, such as trees, river, and a bridge. These outliers were removed by applying a threshold for the elevation at

the 5% significance level. The final filtered image that is used to estimate statistical properties of the snow roughness is shown in Figure 2c, where pink indicates not-a-value pixels.

3. SIMULATION OF RANDOM FIELD

In this section, several methods for random field synthesis are considered and evaluated from a practical point of view. The evaluation of the methods here is based not only on their ability to re-create realistically looking texture, but their efficiency.

Another aspect that is important for applications is the ability to create both, isotropic and anisotropic textures. For example, for snow roughness on a leveled plane, there is no reasons to assume horizontal anisotropy of snow depths. An isotropic random field would be an appropriate choice for this scenario. However, on the hills or in valleys, random variability in snow depth might be biased by gravity, which makes the texture different depending on whether variations align with the gravity geodesic curve or not. Similarly, in some areas there might be predominant wind patterns that will render snow texture along the wind to be different from those in the cross-wind direction.

Yet another important aspect of the modeling method is spatial periodicity beyond the modeling scene. Indeed, synthesis on the large spatial scales with fine resolution may require serious computational resources, in either time or memory. If a method generates a random filed with periodicity beyond the computational boundaries, then, a simple tiling of this image at every side will increase the simulated area.

Lastly, the simulated scene should preferably exhibit spatial ergodicity properties. This means that statistical properties of the modeled random field should be reproduced in each synthesized image, not only in the ensemble sense, on average, when the number of synthesized images is very large.

Thus, an ideal method should be fast, should reproduce realistic textures for isotropic and anisotropic cases in every image, and, preferably, be periodic beyond the boundaries of the simulated scene.

Therefore, heavy mathematical models and neural networks requiring long, and extensive training were not considered in this study.

3.1. Heuristic approach

One of the simplest methods to generate a random field of snow depth is through a sum of the 2D Gaussians randomly placed in the square simulation area $L \times L$:

$$H(\mathbf{r}) = A \sum_{i=1}^{G} h_i \exp\left[-\frac{(\mathbf{r}-\boldsymbol{\varepsilon}_i)^2}{a^2}\right], \qquad (1)$$

where $H(\mathbf{r})$ is the snow depth at a spatial location $\mathbf{r} = (x, y)$, $0 \le x \le L$, $0 \le y \le L$, G is the number of Gaussians, $h_i = \pm 1$ is a random variable which can take the values of +1 or -1 with equal probability, a is a parameter determining the special scale of variations, $\boldsymbol{\varepsilon}_i = (x_{0i}, y_{0i})$ is a vector of the ith Gaussian center, randomly placed within the simulation area with the uniform probability distribution, and A is a scaling constant, which can be chosen so that the variance of the field $H(\mathbf{r})$ equals the variance of the actual natural scene. The model in Equation (1) can be easily generalized to include anisotropy by allowing different scale parameters a_x and a_y along the x- and y- directions. Figure 3 shows examples of isotropic and anisotropic fields generated by the Gaussian model with various scale parameters.

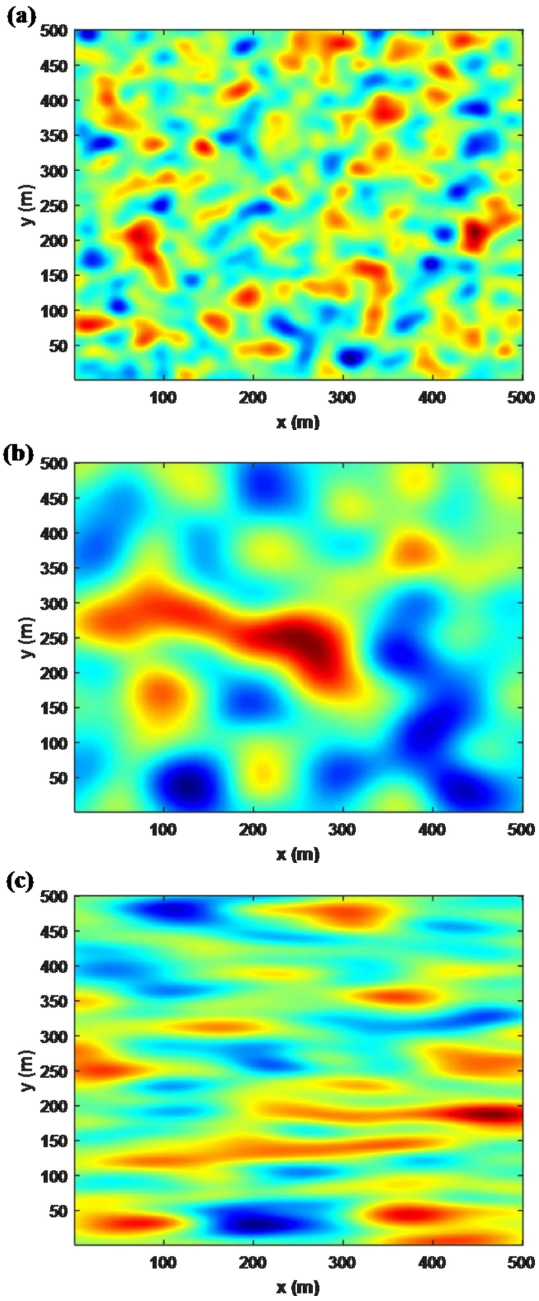

Figure 3: Examples of random fields simulated by the Gaussian model. (a) Isotropic field: $\boldsymbol{a_x = a_y = 10}$ m. (b) Isotropic field: $\boldsymbol{a_x = a_y = 30}$ m. (c) Anisotropic field: $\boldsymbol{a_x = 40}$ m, $\boldsymbol{a_y = 10}$ m.

Advantages of the Gaussian model are its simplicity and computational efficiency. Large spatial scenes can be simulated very quickly. However, the resulting filed may not be quite realistic. By appearance, one can see from Figure 3 that all variations bear somewhat smooth character, which differs from the actual scene depicted in Figure 2c. Moreover, it can be shown that the correlation function of the resulting fields of the Gaussian model is the Gaussian function, while the real scene is best described by the exponential function, as will be shown in the next section. Also, the Gaussian model doesn't have spatial periodicity.

The basic Gaussian model has a quite sophisticated generalization to the quasi-wavelet random field simulation model [9], which can be set up so that it will match a given correlation function. The quasi-wavelet model aims at reproducing a natural way of random field creation, which often follows the principle of self-similarity, resulting in fractal structures. This is achieved by carefully selecting spatial scales of the Gaussian functions, following self-similar scale ratios. Starting with a few parent Gaussians, randomly placed in the simulation area, and applying the scaling principle, the resulting field is found as a sum of all functions of all scales. This quasi-wavelet model has some advantages, such as being able to adjust for a given correlation function and reproduce intermittency in the random fields, but it suffers from the same round edges as the basic Gaussian model, and is not easily generalizable to the anisotropic case. Besides, spatial ergodicity is not guaranteed.

3.2. Random field simulation through the Cholesky decomposition

One common method for random field generation is through the Cholesky decomposition of the covariance matrix [10, 11]. The theory of this technique is based on the observation that a random field with a given covariance can be generated from a delta-correlated random field by a linear superposition of its samples. Indeed, let $\mathbf{f}$ be a column-vector of independent zero-mean random values (for example, normally distributed), which are delta-correlated:

$$\langle f_i f_j \rangle = \delta_{ij}, \qquad (2)$$

where indices i and j denote the vector elements, $\langle\cdot\rangle$ stands for the mathematical expectation, and δ_{ij} is the Kronecker delta-symbol:

$$\delta_{ij} = \begin{cases} 1, & i = j \\ 0, & i \neq j \end{cases}. \qquad (3)$$

Another random variable, a column-vector $\mathbf{s}$, can be constructed such that each of its element are a linear combination of samples in vector $\mathbf{f}$:

$$\mathbf{s} = \mathbf{W}\mathbf{f}, \qquad (4)$$

where $\mathbf{W}$ is a matrix of weights. The objective is to determine matrix $\mathbf{W}$ so that $\mathbf{s}$ has the desired covariance properties estimated from the experimental data:

$$\langle s_i s_j \rangle = c_{ij}, \qquad (5)$$

where c_{ij} is the covariance estimated from the experimental data. In matrix terms, Equation (5) reads:

$$\langle \mathbf{s}\mathbf{s}^T \rangle = \mathbf{C}, \qquad (6)$$

where $\mathbf{C}$ is the covariance matrix between all elements in $\mathbf{s}$, and the superscript T stands for matrix transpose. Substituting Equation (4) into Equation (6) and noting that $\langle \mathbf{f}\mathbf{f}^T \rangle = \mathbf{I}$ one finds the following condition for the sought matrix $\mathbf{W}$:

$$\mathbf{W}\mathbf{W}^T = \mathbf{C}, \qquad (7)$$

which is solved by the Cholesky decomposition of matrix $\mathbf{C}$.

To apply this technique to the 2D case, first, the empirical covariance function is estimated directly from the data shown in Figure 2c. Figure 4a shows the empirical covariance function under assumptions of spatial homogeneity and isotropy of the snow depth variations (blued curve), which are justified for the leveled terrain. As one can see, the empirical covariance is very well described by the fitted exponential covariance function (red dashed curve).

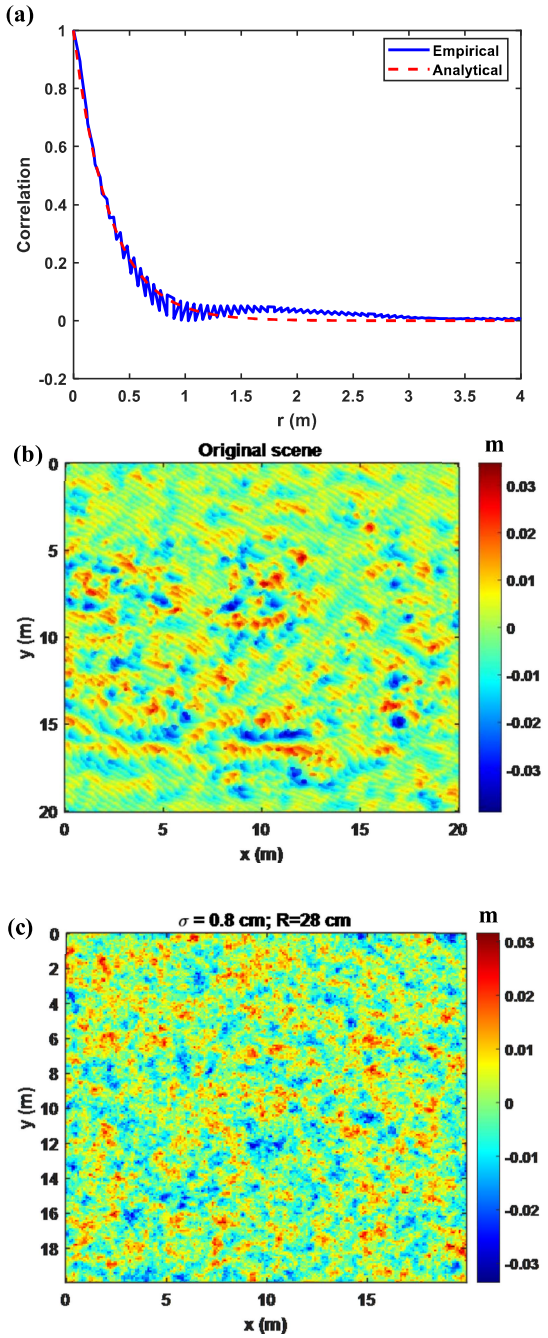

Figure 4: Simulation of the random snow height variations by the Cholesky technique. (a) The empirical and analytical covariance function for the data shown in Figure 2c. (b) A

patch of 20 m by 20 m from Figure 2(c). (c) Synthetic filed to represent the scene in Figure 4b.

Then, samples from a 2D spatial grid with a spatial resolution of 10 cm and the simulation size of 20 m by 20 m are straightened into a single vector **s**, and the covariance matrix **C** is calculated using the fitted exponential function. Figures 4b and 4c show a 20 m by 20 m patch from the actual data shown in Figure 2c, and the simulated random field, respectively. Comparing these two figures, one can see that the amplitude and characteristic scales of spatial variations are reproduced sufficiently accurately. Also, the covariance function was estimated using the entire image in Figure 2c, while only a single patch is shown in Figure 4b, which may have somewhat different statistical properties.

The drawbacks of this approach lie in its limited efficiency in the case of large spatial scales. Indeed, if there are M samples along each dimension, the covariance matrix has the dimension of $M^2 \times M^2$. In the example in Figure 4, which uses 10 cm resolution for a scene with 20 m side length, the covariance matrix has the dimension of 40,000 by 40,000. For practical applications, even larger scenes might be of interest. The Cholesky decomposition of such large matrices becomes time and memory intensive to operate, which is a recognized deficiency of this approach [12]. Another aspect is that the simulated scene is not periodic in space.

Another sampling approach that was tried out and which does not require the Cholesky decomposition is sampling from the multivariate correlated normal distribution, provided by the "lhsnorm" function in Matlab. This approach treats every sample in the simulated field as a dimension of a space, and, as such, can be sampled from a multidimensional normal distribution with a given covariance matrix between all samples, **C**. However, the application of this approach did not produce satisfactory results, as there is not guarantee that a single synthesized image possesses desirable statistical properties.

3.3. Random filed simulation using the Wiener–Khinchin theorem.

The method considered in this section is the FFT-MA method [13, 14] implemented in the frequency domain, which substantially improves efficiency by avoiding 2D convolution. The Wiener–Khinchin theorem states that the power spectral density equals the Fourier transform of the correlation function (if such a transform is feasible). For many analytical correlation functions, this transform exists in a strict mathematical sense. Moreover, for a finite length of the correlation function and simulation scenes, the *discrete* Fourier transform always exists. This is sufficient for the intended application. For a homogeneous random field, the theorem states:

$$P(\mathbf{k}) = \int_{-\infty}^{\infty} B(\boldsymbol{\rho}) \exp(-i\mathbf{k}\boldsymbol{\rho}) d\boldsymbol{\rho}, \qquad (8)$$

where $\mathbf{k} = (k_x, k_y)$ is a wave vector, $\boldsymbol{\rho} = \mathbf{r}_1 - \mathbf{r}_2 = (\rho_x, \rho_y)$ is a separation vector between two spatial locations, P is the power spectral density, and B is the covariance function.

As one can see in Figure 4a, the covariance function for snow depth variation is described by the exponential function:

$$B(\boldsymbol{\rho}) = \sigma^2 \exp\left(-\frac{\rho}{b}\right), \qquad (9)$$

where σ^2 is the variance, $\rho = |\boldsymbol{\rho}|$, and b is the correlation radius. For such a function, Equation 8 can be evaluated analytically:

$$P(\mathbf{k}) = P(k) = \frac{\sigma^2 b^2}{(1+b^2 k^2)^{3/2}}, \qquad (10)$$

where $k = |\mathbf{k}| = \sqrt{k_x^2 + k_y^2}$.

On the other hand, it can be shown that the Fourier transform of a random field with desired correlation properties equals the product of the spatial spectra of the square root of the power spectral density and the delta-correlated random field [13]. Therefore:

$$z(\mathbf{r}) = \frac{1}{(2\pi)^2}\int_{-\infty}^{\infty} p(\mathbf{k})\exp(i\mathbf{kr})d\mathbf{k}, \quad (11)$$

where $z(\mathbf{r})$ is the sought field of snow height,

$$p(\mathbf{k}) = \sqrt{P(k)}Q(\mathbf{k}), \quad (12)$$

and $Q(\mathbf{k})$ is the 2D Fourier transform of an independent normally distributed random field, which can be modeled as a unit-magnitude, random phase, complex quantity. The mean-centered variations are obtained by removing the spatial mean of $z(\mathbf{r})$ over the scene.

Figure 5 shows an example of random snow height realizations for two spatial scales, 0.28 m and 1 m correlation radii.

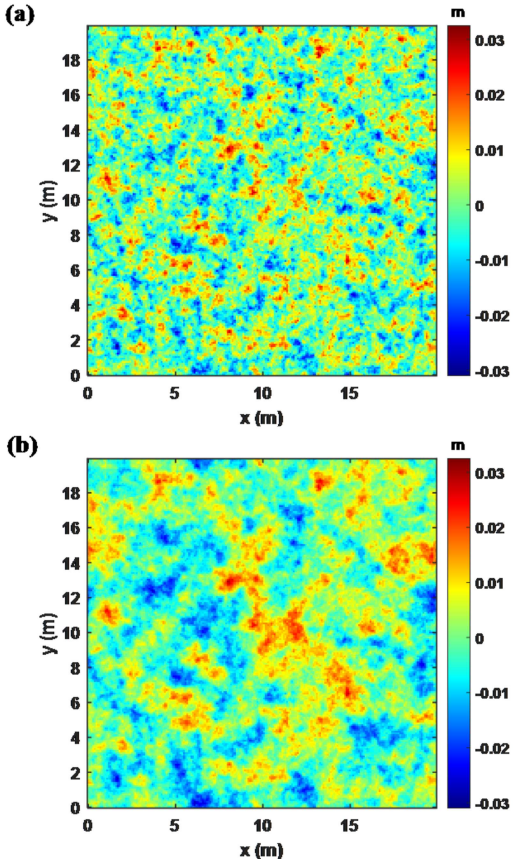

Figure 5: Snow scene generated by the Wiener–Khinchin technique. (a) Correlation length is 0.28 m. (b) Correlation length is 1 m.

This approach can accommodate the anisotropic case by prescribing different spatial scales for the x- and y-directions. Likewise, it can accommodate various covariance functions.

One advantage of this method is its computational efficiency. Note that there is no need in covariance matrix computation, matrix inversion, and the Cholesky decomposition. The fast inverse Fourier transform implemented numerically in Equation 11 has the $N\log N$ efficiency (N being the total number of samples in the simulated field) and works very fast even for relatively large numerical arrays.

Another advantage is that the generated scenes are periodic beyond their boundaries, allowing one to tile the same scene to obtain a realistic representation for a larger area. For example, Figure 6 shows a large scene created by tiling together 9 scenes shown in Figure 5a, which produces a 60 m by 60 m scene with no discontinuities and minimal additional effort.

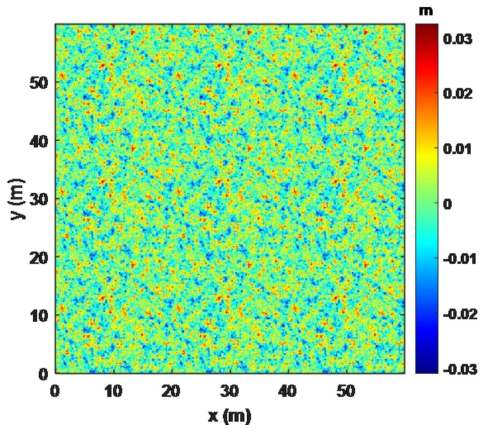

Figure 6: Tiling a scene shown in Figure 5a to produce a larger scene of 60 m by 60 m using the field periodicity over the boundaries.

4. CONCLUSIONS

In order to develop a robust fully autonomous off-road technology, numerical simulations are often used in the developmental stage. However, the meaningful conclusions from such efforts require realistic specification of natural terrain properties. One specific aspect of such realistic terrain specification is modeling snow scene texture to

adequately predict sensor performance for terrain classification. This will allow for a design of more intelligent, terrain-informed autonomous systems.

In this paper, the snow height field obtained for an experimental site through photogrammetry is decomposed on the background and random field components, based on the user-defined outer and inner spatial scales. The scale parameters were used as input for random field simulations that describe snow texture. Several common approaches were considered, such as Gaussian model, Cholesky decomposition technique, and the FFT-MA method based on the Wiener-Khinchin theorem.

The simulation results were evaluated using multiple metrics, such as realistic texture representation, numerical efficiency, ability to handle isotropic and anisotropic scenarios, and ability to produce larger spatial scenes by tiling together a small simulated area without discontinuities. The results indicate that the overall best method that satisfies all the metrics is FFT-MA method, while the Cholesky decomposition technique is the second best.

5. ACKNOWLEDGEMENTS

This study was conducted for the U.S. Army Corps of Engineers under Simulation Tools For CoVeR PE 622145 / Project BG2 / Task 03, “UE4 Winter Scene Generation.” The permission to publish has been granted by the Director, Cold Regions Research and Engineering Laboratory.

6. REFERENCES

[1] M. Parker et al., "Exploring cold regions autonomous operations," Journal of Terramechanics, vol. 96, pp. 159-165, 2021.

[2] O. Welling, A. Meyer, S. Vecherin, and M. Parker, "Determining Where a Vehicle Can and Cannot Safely Drive," in Ground Vehicle Systems Engineering and Technology Symposium (GVSETS), NDIA, Novi, MI, 2021, pp. 1-12.

[3] Mitchell, K. E., "The Community Noah Land Surface Model (LSM)—user’s guide (v2.2)," ed, 2001.

[4] Mitchell, K. E., "The multi-institution North American Land Data Assimilation System (NLDAS): Utilizing multiple GCIP products and partners in a continental distributed hydrological modeling system," vol. 109, ed, 2004, p. D07S90.

[5] D. G. Tarboton and C. H. Luce, Utah energy balance snow accumulation and melt model (UEB). Citeseer, 1996.

[6] J. Pomeroy, D. Gray, and P. Landine, "The prairie blowing snow model: characteristics, validation, operation," Journal of Hydrology, vol. 144, no. 1-4, pp. 165-192, 1993.

[7] G. E. Liston and K. Elder, "A distributed snow-evolution modeling system (SnowModel)," Journal of Hydrometeorology, vol. 7, no. 6, pp. 1259-1276, 2006.

[8] M. Nolte, N. Kister, and M. Maurer, "Assessment of deep convolutional neural networks for road surface classification," in 2018 21st International Conference on Intelligent Transportation Systems (ITSC), 2018: IEEE, pp. 381-386.

[9] G. H. Goedecke, V. E. Ostashev, D. K. Wilson, and H. J. Auvermann, "Quasi-Wavelet Model of Von Kármán Spectrum of Turbulent Velocity Fluctuations," Boundary-Layer Meteorology, vol. 112, no. 1, pp. 33-56, 2004/07/01 2004, doi: 10.1023/B:BOUN.0000020158.10053.ab.

[10] L.-L. Liu, Y.-M. Cheng, and S.-H. Zhang, "Conditional random field reliability analysis of a cohesion-frictional slope," Computers and Geotechnics, vol. 82, pp. 173-186, 2017.

[11] D.-Q. Li, S.-H. Jiang, Z.-J. Cao, W. Zhou, C.-B. Zhou, and L.-M. Zhang, "A multiple response-surface method for slope reliability analysis considering spatial variability of soil properties," Engineering Geology, vol. 187, pp. 60-72, 2015.

[12] T. Tao, H. Wang, and K. Zhao, "Efficient simulation of fully non-stationary random wind field based on reduced 2D hermite interpolation," Mechanical Systems and Signal Processing, vol. 150, p. 107265, 2021.

[13] D. S. Oliver, "Moving averages for Gaussian simulation in two and three dimensions," Mathematical Geology, vol. 27, no. 8, pp. 939-960, 1995/11/01 1995, doi: 10.1007/BF02091660.

[14] L. P. de Figueiredo, D. Grana, and M. Le Ravalec, "Revisited Formulation and Applications of FFT Moving Average," Mathematical Geosciences, vol. 52, no. 6, pp. 801-816, 2020/08/01 2020, doi: 10.1007/s11004-019-09826-4.